

# Study the Properties of Solution Processable CZTS Thin Films Induced by Annealing Treatment: Study of Annealing Time

R. A. Gani Shaikh<sup>a</sup>, S. A. More<sup>a</sup>, G. G. Bisen<sup>a</sup>, and S. S. Ghosh<sup>a,\*</sup>

<sup>a</sup> Optoelectronics Laboratory, Department of Physics, Kavayitri Bahinabai Chaudhari North Maharashtra University, Jalgaon, Maharashtra, 425001 India

\*e-mail: ssgosh@nmu.ac.in

Received May 13, 2020; revised May 13, 2020; accepted May 21, 2020

**Abstract**—Cu<sub>2</sub>ZnSnS<sub>4</sub> is suitable for high-performance thin-film solar cell because of its high absorbance coefficient, presence of non-toxic elements, excellent optoelectronic properties, and a near-perfect direct band gap. The effect of thermal annealing time (1–4 h) on the optical, morphological, and structural properties of Cu<sub>2</sub>ZnSnS<sub>4</sub> coated through a simple solution processable method has been studied in the present work. All the CZTS films are crystalline in nature with kesterite structure as shown by X-ray diffraction studies. Crystallite size, strain, and dislocation density were calculated. However, no notable changes in these parameters were obtained by varying the annealing time in the above range. Field emission scanning electron microscopy images show good quality compact films with particle size in the order of 10–15 nm. Absorption spectroscopy results show an optical band gap of 1.46 eV. Raman spectroscopy was used to check binary or ternary phases present. It shows that the impurity phase decreases and the pure Cu<sub>2</sub>ZnSnS<sub>4</sub> phase was obtained by increasing the annealing time to 3 and 4 h.

**Keywords:** Cu<sub>2</sub>ZnSnS<sub>4</sub>, thermal annealing, optical, characterization, Raman spectroscopy

**DOI:** 10.1134/S1063782620090110

## 1. INTRODUCTION

In recent years, the worldwide attraction for research in the areas of photovoltaics (PV) has increased, due to challenges like limited availability and serious environmental issues associated with conventional energy sources [1]. In the last decade, progress in thin-film technologies has strongly promoted the second-generation solar cells. Thin-film technologies effectively reduce the cost of material due to the demand for fewer material and solution processability [2]. Besides, thin films can be easily deposited on a substrate like glass, stainless steel, plastic, etc. [3].

There are many thin-films solar-cell technologies available that make use of amorphous silicon, copper indium selenide (CIS), cadmium telluride (CdTe), copper indium gallium selenide (CIGS), gallium arsenide (GaAs) [4]. Solar cells based on the above materials have high light-to-electricity conversion efficiency of ~20% and are comparatively low in cost. However, amorphous silicon is not stable, GaAs and CdTe contain toxic elements like arsenic and cadmium, CIGS contain rare indium, and therefore these type of solar cell materials will not be effective [5]. The search for alternative thin-film technologies is in progress through active research. Currently, the quaternary compound Cu<sub>2</sub>ZnSnS<sub>4</sub> (CZTS) is widely considered as an alternative PV material due to the prop-

erties similar to CIGS. CZTS is a *p*-type semiconductor of groups I<sub>2</sub>–II–IV–VI<sub>4</sub> and has a direct band gap ~1.5 eV. It has high absorption coefficient in the visible region of solar radiation, low cost, absence of toxic elements, and presents in abundance on earth [6]. Since the rare and expensive indium is replaced by cheap and earth-abundant zinc and tin, it is regarded as an alternative to CIS and CIGS materials. Due to many distinguishing characteristics of CZTS, solar cell based on thin-film of this material is the best candidate for low-cost energy generation in the future [7]. CZTS thin film can be synthesized by various non-vacuum or vacuum-based deposition techniques like electrodeposition using ionic liquid, successive ionic layer adsorption and reaction, chemical spray pyrolysis, chemical bath deposition, sol-gel spin coating method, etc. [8]. Vacuum-deposition techniques are complicated, expensive, and non-versatile. Solution-based deposition techniques are attractive because of low-cost deposition, low input energy and effective control over the shape and size of nanocrystals [9]. Thermal annealing the thin films is a common method used to obtain materials with desired phase and properties [10, 11].

In the present work, we have studied the effect of thermal annealing especially focusing on annealing time on the CZTS thin film properties, prepared by a comparatively new sol-gel multiple-layer spin coating

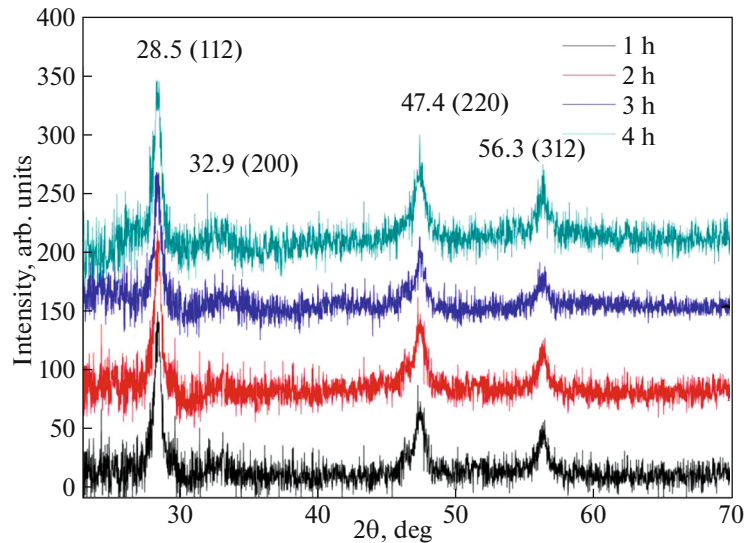


Fig. 1. X-ray diffraction spectra of the different CZTS samples annealed at 300°C for different times.

method. The films have been annealed for different times (1–4 h) and the effect on the optical, morphological, and structural properties has been studied by X-ray diffraction, UV-visible absorption spectroscopy, field emission scanning electron microscopy, and Raman spectroscopy studies. Our studies show that thermal annealing time is critical in removing impurity, and pure CZTS can be formed upon thermal annealing for the optimum time.

## 2. EXPERIMENTAL

CZTS sol–gel precursor solution was synthesized by adopting the following procedure [12]. In the synthesis of 10 mL of CZTS precursor solution, 10 mL dimethylsulfoxide was taken in a 25-mL volume conical flask. Then 0.852 g of  $\text{CuCl}_2 \cdot 2\text{H}_2\text{O}$  (0.5 M) was added in DMSO to get a deep blue solution. Then precursor of 0.564 g of  $\text{SnCl}_2 \cdot 2\text{H}_2\text{O}$  (0.25 M) was added in the flask. The solution was then stirred for 12 h at room temperature, after which the suspension changes color to clear light green. Thereafter, 0.341 g of  $\text{ZnCl}_2$  (0.25 M) was added into the solution, resulting in a solution having a yellow tint. Thereafter, 1.142 g of thiourea (1.5 M) was added. A transparent and colour-

less solution was obtained when thiourea completely dissolves. Finally, 0.058 g of NaCl (0.1 M) was added into the solution. This solution was then spin-coated on the glass substrate. In well-optimized conditions we get a uniform thin film of CZTS material after drying the samples on the preheated hot plate at 200°C for 2 min. This cycle was repeated six times to obtain the desired thickness. After final drying, CZTS films were transferred to muffle furnace to anneal for 1–4 h at 300°C temperature. Thereafter, the films were allowed to cool to room temperature.

X-ray diffractometer (using  $\text{CuK}\alpha$  radiation with  $\lambda = 1.54060 \text{ \AA}$ , Bruker D8 ADVANCE) was used to study the structural properties of the formed CZTS films. Field effect scanning electron microscopy (FESEM) using Hitachi S4822 was used to study the surface morphology of the samples. The optical properties of all samples were measured by UV-visible absorption spectrometer Shimadzu 1601. Raman spectra were recorded by using LABRAM HR-800 single spectrometer equipped with an excitation source 632.8 nm line of He-Ne laser and CCD detector with a spectral resolution  $1 \text{ cm}^{-1}$ .

Table 1. Values of FWHM, crystallite size, dislocation density, and strain in CZTS films annealed for different times

Annealing time, h	$2\theta$ , deg	FWHM	Crystallite size, nm	Dislocation density, $\text{lin}/\text{m}^2$	Strain, $10^{-3} \text{ lin}^{-2} \text{ m}^{-4}$
1	28.5	0.6268	13.7	$5.4 \times 10^{16}$	2.7
2	28.5	0.5974	14.3	$5.2 \times 10^{16}$	2.6
3	28.5	0.6287	13.9	$5.4 \times 10^{16}$	2.7
4	28.4	0.6152	13.6	$4.9 \times 10^{16}$	2.5

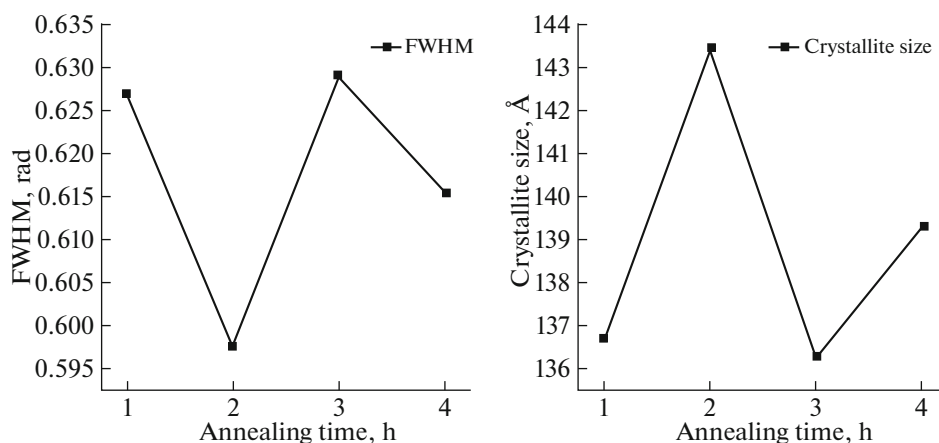


Fig. 2. Crystallite size and FWHM of CZTS films grown by sol-gel spin coating method.

### 3. RESULTS AND DISCUSSION

#### 3.1. X-Ray Diffraction Study

X-ray diffraction pattern of the CZTS films annealed at 300°C for different times is shown in Fig. 1.

X-ray diffraction patterns of the films were recorded in the  $2\theta$  range  $20^\circ$  to  $70^\circ$ . The crystallite size  $D$ , strain  $\varepsilon$ , and the dislocation density  $\delta$  were calculated by using the following formula [13]:

$$D = \left( \frac{0.94\lambda}{\beta \cos \theta} \right),$$

$$\varepsilon = \frac{\beta \cos \theta}{4},$$

$$\delta = \left( \frac{1}{D^2} \right),$$

where  $\beta$  is the full width at half maximum (FWHM). From the X-ray diffraction pattern, it is revealed that for all CZTS samples characteristics peaks were observed at  $28.5^\circ$ ,  $32.9^\circ$ ,  $47.4^\circ$ , and  $56.3^\circ$  values of  $2\theta$ . These are attributed to the (112), (200), (220), and (312) planes, respectively, and matches with the JCPDS data (26-0575). It confirms the kesterite structure of the CZTS thin films. Crystallites have a preferential orientation in the (112) plane direction and have a tetragonal phase [14]. The sharp peak for (112) orientation is due to crystalline nature in the material. The calculated values of FWHM, crystallite size, dislocation density, and strain are shown in Table 1.

However, there was no clear trend observed with variation in annealing time in all these quantities. The crystallite size calculated was in the range 13.5 to 14.5 nm. This indicates that the effect of annealing time from 1–4 h does not have a significant effect on the CZTS structure. Also a significant effect on the defects in the films was not observed. The variations of FWHM and crystallite size with annealing time are as shown in Fig. 2.

#### 3.2. Film Morphology and Optical Properties

Particle size and morphology mainly depends upon the annealing parameters and the composition of the film. Figure 3 shows the FE-SEM micrograph of CZTS films annealed at 300°C for different times.

Effect of annealing time on the morphology both at the nanoscale and micrometer scale was studied. Upon increasing the annealing time, the particle size was not affected. The particle size observed was 10–15 nm for all the films. It was obvious that the surface morphology of all the films is smooth and uniform with very few cracks. At the micrometer scale also the film annealed for 1 h is smooth, and larger features were not visible in the films. Further, as the annealing time increases to 2 h, larger particles were seen in the film. This is due to the growth of some of the particles in the films. This is consistent with XRD results. Upon

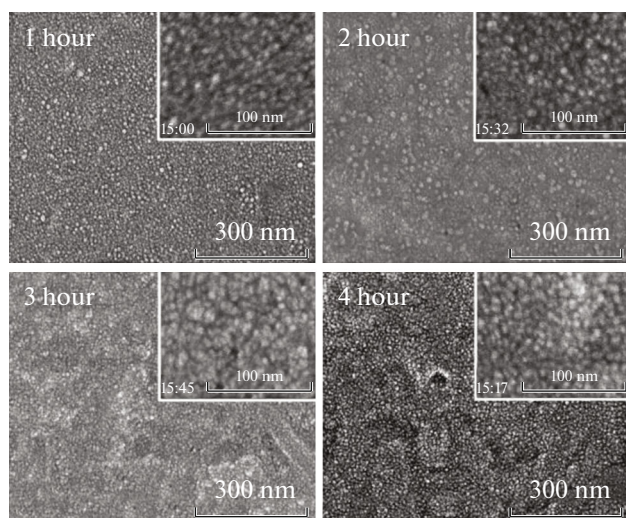


Fig. 3. FESEM images of the CZTS films annealed at 300°C for different times.

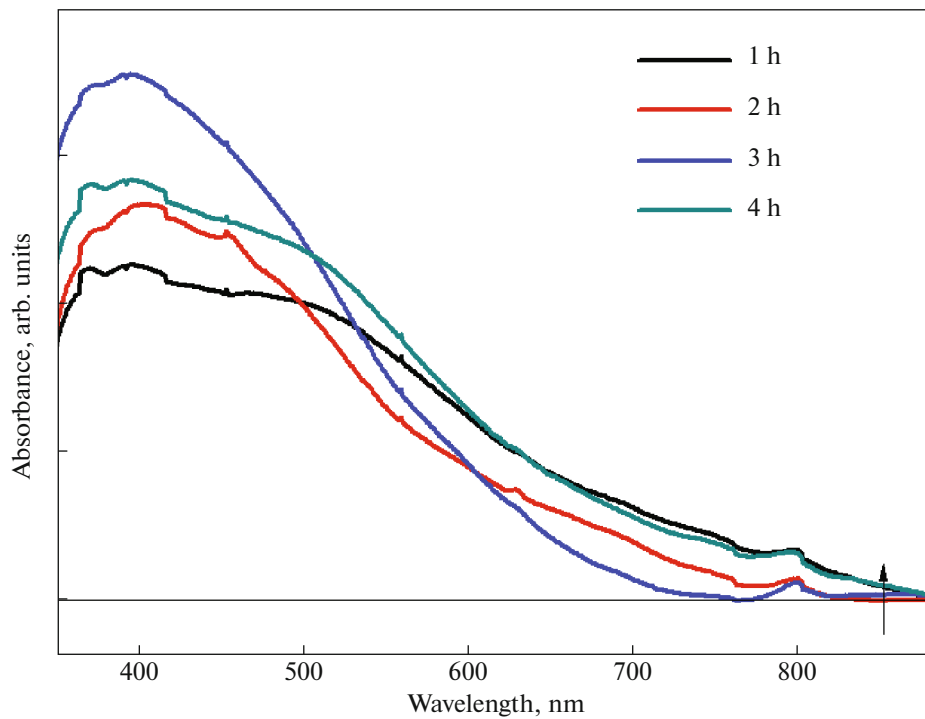


Fig. 4. UV-visible absorption spectra of the CZTS samples annealed at 300°C for different times.

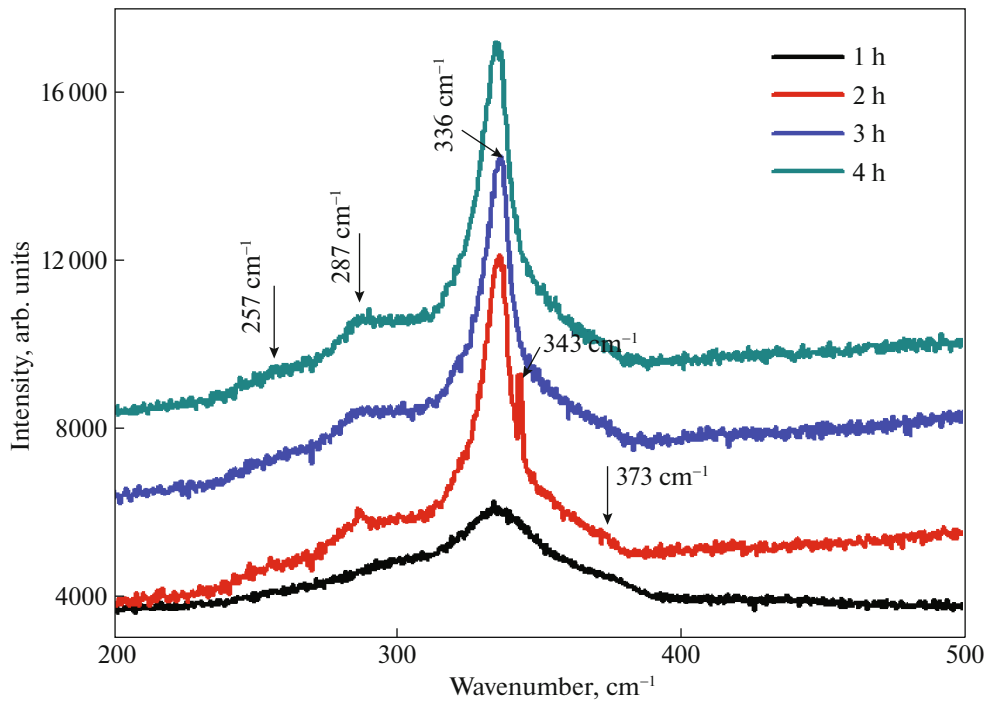


Fig. 5. Raman spectra of the CZTS samples annealed at 300°C for different times.

annealing for 3 h, a large contrast was observed between different regions of the film and the film appeared rough. Upon annealing for 4 h, such features were also seen.

Figure 4 shows the absorption spectra of the CZTS films annealed for different times.

Absorption onset for all the annealed samples is near the 850 nm suggesting an optical band gap of

1.46 eV. Broadly, the absorption coefficient increases with a decrease in wavelength. This is consistent with the already reported literature [15, 16].

### 3.3. Raman Spectroscopy

Figure 5 shows the Raman spectra of CZTS films annealed at 300°C for different times.

Excitation was performed with 632-nm wavelength to confirm the phase purity of samples. It is important to acknowledge that XRD is singly insufficient to determine the phase purity of the CZTS films [17, 18]. The Raman spectra show high intense peaks at 336  $\text{cm}^{-1}$  and a comparatively less intense peak at 287  $\text{cm}^{-1}$  consistent with previously reported values for CZTS material [19, 20]. These peaks are corresponding to the  $A_1$  mode due to the vibration of S atoms surrounded by motionless neighboring atoms. The intensity of these peaks is, however, less for the film annealed for 1 hour, and it increases by increasing the annealing time. This is an indication of enhanced crystallization after annealing for 2 h and more. The peaks at 257 and 287  $\text{cm}^{-1}$  are also attributed to the CZTS kesterite phase [21]. A less intense shoulder peak was observed at 343  $\text{cm}^{-1}$  upon annealing for 1 hour. This is attributed to the  $\text{Cu}_3\text{SnS}_4$  phase [22]. The intensity of this peak increases upon annealing for 2 h. Upon annealing for longer times, however, this peak disappears indicating the time-dependent phase transformation towards the formation of pure CZTS. This suggests that good phase of CZTS in the films is formed upon annealing for 3 and 4 h of annealing times.

### CONCLUSIONS

We have reported the effect of thermal annealing time on the CZTS film properties prepared by sol-gel spin coating method on glass substrates. CZTS samples annealed for 1, 2, 3, and 4 h. CZTS film annealed at 300°C for different times show the kesterite phase in all the samples. Raman spectroscopy results show the presence of  $\text{Cu}_3\text{SnS}_4$  upon annealing for 1 and 2 h. The content of this impurity decreases upon increasing the annealing time. Thermal annealing time is therefore a critical factor for obtaining pure CZTS films.

### ACKNOWLEDGMENTS

The authors are thankful to Dr. Vasant Sathe and UGC-DAE Consortium for Scientific Research for doing Raman spectroscopy measurements.

### CONFLICT OF INTEREST

Authors have no conflict of interest to be declared.

### REFERENCES

1. M. Pagliaro, R. Ciriminna, and G. Palmisano, *ChemSusChem* **1**, 880 (2008).
2. T. M. Gadzhiev, M. A. Aliev, A. S. Asvarov, R. M. Gadzhieva, and B. A. Bilalov, *Semiconductors* **53**, 1992 (2019).
3. X. Song, X. Ji, M. Li, W. Lin, X. Luo, and H. Zhang, *Int. J. Photoenergy* **1**, 613173 (2014).
4. M. A. Green, E. D. Dunlop, J. H. Ebinger, M. Yoshita, N. Kopidakis, and A. W. Y. H. Baillie, *Prog. Photovolt. Res. Appl.* **28**, 3 (2020).
5. P. S. Shinde, C. A. Betty, P. N. Bhosale, Y. Woo, and P. S. Patil, *J. Phys. Chem. Solids* **73**, 735 (2012).
6. H. Katagiri, K. Saitoh, T. Washio, H. Shinohara, T. Kurumadani, and S. Miyajima, *Sol. Energy Mater. Sol. Cells* **65**, 141 (2001).
7. B. Shin, O. Gunawan, Y. Zhu, N. A. Bojarczuk, S. J. Chey, and S. Guha, *Prog. Photovolt. Res. Appl.* **21**, 72 (2013).
8. K. Tanaka, M. Oonuki, N. Moritake, and H. Uchiki, *Sol. Energy Mater. Sol. Cells* **93**, 583 (2009).
9. H. Zhou, W. Hsu, H. Duan, B. Bob, and W. Yang, *Energy Environ. Sci.* **6**, 2822 (2013).
10. S. W. Shin, J. H. Han, Y. C. Park, G. L. Agawane, C. H. Jeong, J. H. Yun, A. V. Moholkar, J. Y. Lee, and J. H. Kim, *J. Mater. Chem.* **22**, 21727 (2012).
11. L. Chen and C. Park, *Korean J. Chem. Eng.* **34**, 1187 (2017).
12. R. Chen, J. Fan, C. Liu, X. Zhang, Y. Shen, and Y. Mai, *Sci. Rep.* **6**, 35300 (2016).
13. S. Lalitha, R. Sathyamoorthy, S. Senthilarasu, A. Subbarayan, and K. Natarajan, *Sol. Energy Mater. Sol. Cells* **82**, 187 (2004).
14. M. C. Benachour, R. Bensaha, and R. Moreno, *Optik* **187**, 1 (2019).
15. D. Lee and K. Yong, *ACS Appl. Mater. Interfaces* **4**, 6758 (2012).
16. B. Flynn, W. Wang, C. Chang, and G. S. Herman, *Phys. Status Solidi A* **209**, 2186 (2012).
17. Q. Guo, G. M. Ford, W. Yang, B. C. Walker, E. A. Stach, H. W. Hillhouse, and R. Agrawal, *J. Am. Chem. Soc.* **132**, 17384 (2010).
18. K. Wang, B. Shin, K. B. Reuter, T. Todorov, and D. B. Mitzi, *Appl. Phys. Lett.* **98**, 051912 (2011).
19. T. Shiyani, D. Raval, M. Patel, I. Mukhopadhyay, and A. Ray, *Mater. Chem. Phys.* **171**, 63 (2016).
20. B. Jheng, P. Liu, and M. Wu, *Sol. Energy Mater. Sol. Cells* **128**, 275 (2014).
21. G. D. Teterina, V. N. Nevolin, I. P. Sipaylo, S. S. Medvedeva, and P. E. Teterin, *Semiconductors* **50**, 549 (2016).
22. P. A. Fernandes, P. M. P. Salomé, and A. F. da Cunha, *Phys. Status Solidi C* **7**, 901 (2010).